Architectural Features and Urban Propagation

Antonis G. Dimitriou, *Student Member, IEEE,* and George D. Sergiadis, *Member, IEEE*

***Abstract*—Radiocoverage measurements in urban environments often unveil unexpected power distribution patterns. Architectural features seem to be the cause of this behavior, as demonstrated in this paper. We demonstrate that the elements of a typical building facade, such as windows, exterior doors, balconies and railings, should be considered as significant "sources" of EM radiation in several current wireless communication systems. We propose a method for modeling the influence of those scatterers in EM wave propagation. In our model, the major structural elements are represented by two sets of orthogonally arranged wedges. The uniform geometrical theory of diffraction is employed to calculate the scattering field. The simulation results show that such "urban" scatterers may create a dominant propagation mode in an urban canyon. Our predictions are additionally verified by experimental measurements, performed at two different sites. Finally, the influence of roadside foliage is investigated and conclusions are drawn on the resultant field.**

***Index Terms*—Diffraction, propagation modeling, radiocoverage, ray tracing, urban areas, uniform geometrical theory of diffraction (UTD).**

I. Introduction

REVEALING the properties of urban propagation conditions has been of great interest, due to the flourishing development of modern wireless communication applications. The last years, computer power allowed the evolution from empirical and semi-deterministic propagation prediction models to more sophisticated ones, based mainly on a combination of ray-tracing and uniform theory of diffraction (UTD). The latter offers a well-defined mathematical layout for the description of multiple paths between receivers and transmitters for a site specific environment. These models were successfully applied in the indoor channel, [1], [2], and are currently used also in the urban scene, especially for microcellular communications having a coverage radius of less than 1 km, [3], [4]. For a complete list of all relevant models we refer the interesting reader to [5].

In the case of urban propagation prediction, all the above models consider only the major structural elements of the environment such as whole buildings or even entire blocks. Therefore, they fail to account for the influence of numerous other scattering elements between the receiver and the transmitter, such as cars, traffic lights or openings along the facades of the buildings.

In a better approach, the buildings are considered as having sharp corners and partially rough surfaces. In such a case, part of the incident energy is scattered to all directions. This assumption however, leads to uncertain conclusions, since it neglects the mentioned numerous urban scatterers.

Fig. 1. View of a typical building layout in Thessaloniki, Greece.

We attempt to overcome these limitations and provide a further insight on the mechanisms that drive propagation in the urban environment, by deconstructing the major structural elements, such as the buildings, into appropriate smaller objects and then employ the UTD for the investigation of their scattering behavior in the wireless channel. In general, two types of scattering elements are identified with respect to the temporal variation of their influence; nonstatic, such as cars and pedestrians and static. The latter are mainly "anomalies" along the facades of the buildings, or independent structures, such as street lamps, signs and traffic lights.

In this paper, we attempt to examine the effects caused by static scatterers located along the buildings' facades. A typical "Mediterranean" building structure is shown in Fig. 1. Examples of such scatterers are balconies, rows of railings, windows and exterior doors. Their influence becomes more significant as the frequency increases and thus this analysis becomes more important for the development of new telecommunication systems, usually at higher frequencies, due to the spectrum scarcity.

The concept behind the proposed analysis is briefly explained in Fig. 2. A single floor of the typical building is represented in Fig. 2(a). All its perpendicular scatterers are considered as wedges, as shown in Fig. 2(b). We follow a similar procedure for the scatterers with axes parallel to the ground, and finally we represent the entire facade with two orthogonal sets of wedges, as shown in Fig. 3. The interaction of the incident field with all the wedges is calculated, based on the UTD formulas. The total field is then appropriately derived as the sum of the above interactions. The basic idea in details is presented in Section II. In Section III, all the necessary mathematical background and some important physical properties of the diffraction coefficient formula is provided. In Section IV, the influence of the scatterers in various typical urban configurations is evaluated. In

Manuscript received March 21, 2005; revised November 16, 2005.

The authors are with the Aristotle University of Thessaloniki, School of Engineering, Department of Electrical and Computer Engineering, Telecommunications Laboratory, Thessaloniki GR-54124, Greece (e-mail: antodimi@mri.ee.auth.gr; sergiadi@auth.gr).

Digital Object Identifier 10.1109/TAP.2006.869919

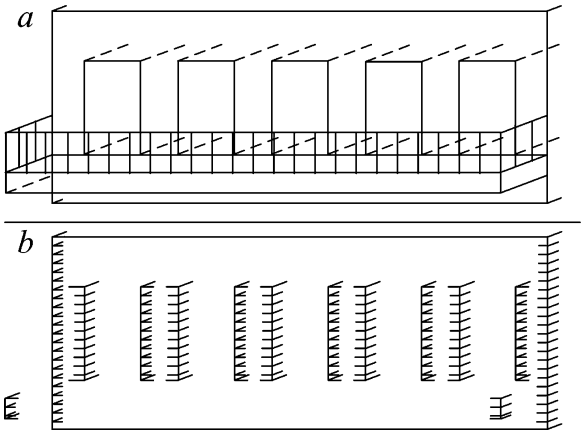

Fig. 2. (a) Representation of a single floor of a typical building. (b) Demonstration of the floor's wedges with axes vertical to the ground.

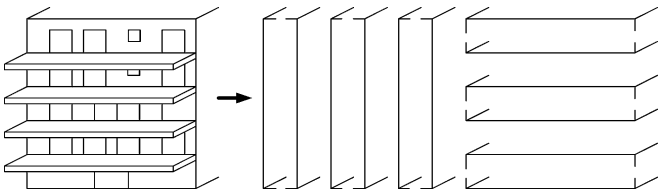

Fig. 3. Representation of the building's surface with two vertically arranged series of wedges, following the procedure demonstrated in Fig. 2.

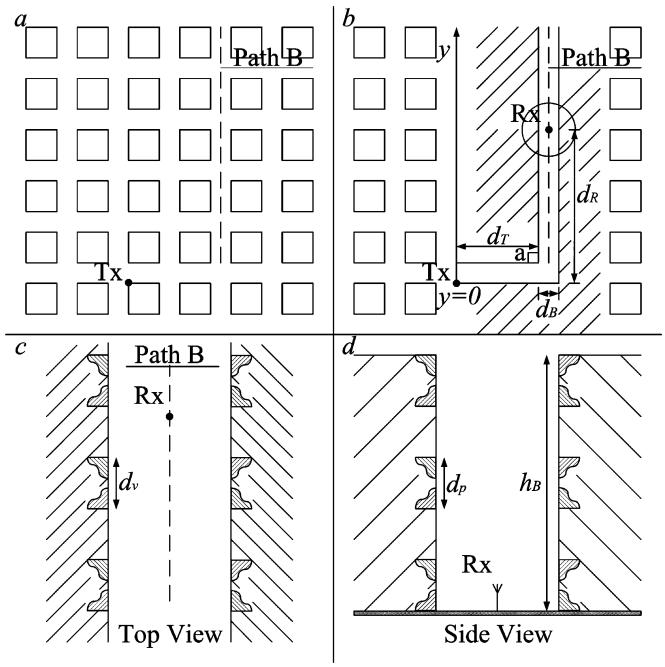

Fig. 4. Schematic representation of the simulation scenario. (a) Typical urban layout. (b) Substitution of the buildings surrounding path B with a continuous structure. (c) Magnified top view of the circular area that surrounds the receiver, where the wedges with axes perpendicular to the ground are shown. (d) Magnified side view of the circular area surrounding the receiver, where the wedges with axes parallel to the ground are shown.

Section V, experimental results at two typical urban canyons validate our predictions. Finally, the conclusions are given in Section VI.

II. Geometrical Formulation

A. Representing the Buildings' Facades With Two Sets of Wedges

When modeling the urban environment, it is pointless to implement a detailed representation of the scene. Even if such a description was at hand, it would be very difficult to appropriately account for the influence of all the existing elements on the propagating waves. Therefore, the model should be derived in a subtractive approach. The most important properties of the scene have to be included, both architecturally and propagation wise. Our aim is therefore to develop a model that takes into account the specific style of the urban scene in a simplified manner, and assigns all the suitable electromagnetic parameters to the structures.

We propose therefore to decompile a building into a more "descriptive" structure, by replacing its facade with two sets of wedges. The first set comprises wedges with axes parallel to the ground, along the facade of the building, substituting the corresponding elements, as shown in Fig. 3 [see also Fig. 4(d)]. The second set of wedges contains the structures that are perpendicular [see Figs. 2 and 3]. In the proposed approach, the wedges are considered continuous along the facade of a building, arranged from the ground to the top of it; an assumption that approximates the actual configuration. This assumption accelerates the calculations in a ray-tracing based radio planning tool, and is not expected to diminish significantly the accuracy of the predictions if the wedge-spacing is properly selected, as will be shown.

The size of the scatterers compared to the wavelength of the transmitted signal is important for the validity of the UTD. However, typical structures have dimensions of at least 2 m; that is many wavelengths longer than most modern communication systems use.

B. Wedge Advantages

Wedges model different existing geometries in a unified manner.

- Windows, doors and other discontinuities along a building's facade can be efficiently approximated by wedges of orthogonal interior angles.
- Railings, or other thin scatterers typically located along balconies, can be replaced by a set of wedges with small or zero interior angles.

Apart from the geometrical similarity of the wedges with the majority of the expected scattering objects, their effects on a propagating EM wave have been thoroughly studied in the past and can be well accounted for in a ray-tracing tool.

C. Pattern of the Scatterers Along the Building's Facade

Observing most buildings' facades, doors and windows are usually arranged in a symmetrical repetitive pattern at fixed relative distances. Therefore, selecting a uniform repetitive pattern of scatterers along a building's facade is considered to be an acceptable approximation.

III. Mathematical Formulation

Geometrical optics (GO) was originally developed to describe the propagation of light. It is based on the consideration of rays emanating from the transmitter to the surrounding environment and interacting with the existing scatterers through reflection and refraction. The geometrical theory of diffraction (GTD), introduced by Keller in 1962 [6], extended the GO by introducing the diffracted rays. Kouyoumjian and Pathak [7] corrected the discontinuities that were predicted by Keller along the shadow boundaries for the case of a perfectly conducting wedge. Burnside with Burgener [8] and then Luebbers [9] proposed an extension of the UTD formula for the inclusion of nonperfectly conducting surfaces.

A. Single Diffraction

The diffracted field $E^d(R_x)$ by a single wedge W, calculated at the receiver R_x at a distance s from the wedge is given by

$$E^d(R_x) = E^i(W)D(W)A(s)e^{-jks} \tag{1}$$

where $E^i(W)$ is the incident field at the wedge, k the propagation constant, $D(W)$ the dyadic diffraction coefficient, and $A(s)$ the spreading factor for diffraction at a wedge, [9]–[11], [25].

The diffraction coefficient generally has two maxima that appear at the corresponding shadow boundary, the incident shadow boundary (ISB) and the reflection shadow boundary (RSB). Around each shadow boundary exists a small angular region, referred to as transition zone, where the intensity of the corresponding coefficient component degrades rapidly. Away from the maxima of the coefficient, the amplitude of the Fresnel transition function is equal to unity. As a result, the corresponding coefficient varies proportionally to the related cotangent.

B. Double Diffraction

Significant research has been carried out for the calculation of the diffracted field by more than a single scatterer. In [10] Bach Andersen considered the contribution of the slope-diffracted field that is generated at each edge, which is considered significant if the subsequent edge is in the transition region of the former one. He introduced a way to calculate the distance parameters L and Ls (for the slope-diffracted field) in order to ensure continuity of the magnitude of the incident field along the successive shadow boundaries. The implementation of Bach Andersen's method is well demonstrated in [11]. In [12] Tzaras and Saunders provided a different methodology for the calculation of the distance parameters in Bach Andersen's method. Each ray path generated at each successive edge has been treated separately, ensuring phase continuity of the fields giving results that match Vogler's solution [13].

In [14], [15], the authors provided a closed-form asymptotic solution for the scattering field by a pair of coplanar skew edges, which was implemented in [16]. In [17], Albani presented an analytic solution for the double diffraction at a pair of perfectly conducting arbitrarily placed wedges.

For a typical double wedge configuration [10]–[12], [18], the diffracted field is calculated using the following set of equations, according to the UTD:

$$\begin{aligned} E_1^d(W_2) &= E^i(W_1)D_1(W_2)A_1(s_1) \\ E_2^d(R_x) &= E_1^d(W_2)D_2(R_x)A_2(s_2) \end{aligned} \tag{2}$$

where W_1, W_2, R_x are the positions of the two wedges and the receiver respectively, $E^i(W_1)$ is the incident field at W_1, $E_i^d(P)$ is the diffracted field by wedge i calculated at point P and $A_i(x)$ denotes the spreading factor, [10], [11], of wedge i, $i = 1, 2$.

To obtain the results presented in the following section, we use (1), (2) for the calculation of the diffracted waves. As it has been shown in [11], [15], [17], the implementation of either the slope-diffraction method [10], [12] or a different approach, [17], [18], becomes important only in the case where successive wedges lay in the shadow boundaries of the previous ones. This is demonstrated through simulation and measurements in [19] for two cases, for which the 2nd wedge is near or exactly at the ISB of the 1st. In our scenarios there are only two wedges involved and the 2nd one is generally not in a SB of the 1st. Therefore, the use of the product of the 1st order diffraction coefficients is expected to be as accurate as the other approaches.

IV. Simulation Results

In order to quantify the magnitude of the effects caused by the described scatterers, we compare their influence on the propagating EM waves with other well known mechanisms. Two cases will be analyzed. In the 1st case, the transmitter is considered well below rooftop level. This is the typical configuration of a microcell, where the antenna is usually placed at a height of 3 m to 12 m. In line-of-sight (LOS) conditions, the received field is characterized by the direct and the multiply reflected rays. In the non-LOS (NLOS) case, the diffracted field from the LOS perpendicular corner is also important [20]–[22].

In the 2nd case, the transmitter is considered above rooftop level. It is well known that the EM waves propagate above the area's roofs and then are diffracted down to the receiver [22]–[24]. They reach the receiving antenna, after being scattered at its vicinity.

In the following analysis, a typical urban building layout is considered, similar to the Manhattan case [22], [25], as shown in Fig. 4(a).

A. Transmitter Placed Below Rooftop Level

In the LOS case, urban propagation is well described by the appropriate summing of the direct and the multiply reflected field components at the receiver. The influence of the diffracted components at the surrounding buildings is expected to be very small compared to the direct one, because of the small magnitude of the corresponding diffraction coefficients. Therefore, the LOS case will not be examined in the following analysis. Let us consider the geometry of Fig. 4(a) and (b). In the case of Fig. 4(b), each row of buildings around path B and the transmitter, is replaced by a continuous structure having height equal to the buildings' (h_B). Our intention is to study all possible

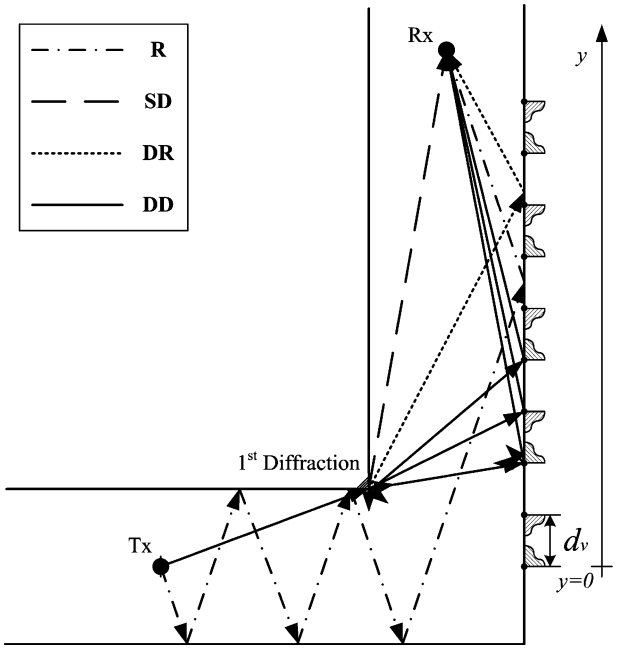

Fig. 5. Representation of the considered propagation mechanisms.

wave-guiding phenomena along path B and compare them with the overall diffracted field from the facades of the buildings.

In order to study the effects caused by the "anomalies" on the buildings (doors, windows, etc.), the surface of the structure around path B is replaced by two sets of orthogonal wedges, following the procedure described in Section II and depicted in Figs. 2 and 3. The magnified top and side views of the area that surrounds the receiver are given in Fig. 4(c) and (d) respectively, to present the two sets of wedges considered. The wedges with perpendicular axes are placed at constant relative distances d_v, while those with axes parallel to the ground at distances d_p. Two alternating patterns of wedges are considered. Each structure, like an opening on a building's facade, a window or a balcony, forms a pair of 90°-wedges (see Fig. 2). Each wedge is examined separately and diffraction is handled as a local phenomenon.

These wedges are made of typical building-construction materials, such as brick or concrete. Railings, typical in Mediterranean cities, were not considered in the simulations, to avoid the focus on the specific architecture. In addition, their dimensions, 40 cm to 60 cm height, are close to the operating wavelength of most modern communications' systems, and their patterns are usually irregular. Therefore, their influence is not estimated to be dominant at the current communications' systems.

For the geometry of Fig. 4(b), the following propagation mechanisms are analyzed along path B (Fig. 5):

a) singly diffracted (SD) ray at corner a;
b) multiply reflected rays (R) in the urban canyon that includes both the transmitter and the receiver;
c) diffracted at corner a, then multiply reflected in the area surrounding path B (DR);
d) doubly diffracted rays (DD) that reach the receiver after being initially diffracted at wedge a and then at each one of the series of the perpendicular wedges at the buildings' facade at the right of path B, as shown in Fig. 5.

TABLE I
DESCRIPTION OF THE ACRONYMS

Symbol	Description of the corresponding propagation mechanism
R	multiple reflections
SD	single diffraction
DR	single diffraction and then multiple reflections
DD	double diffraction

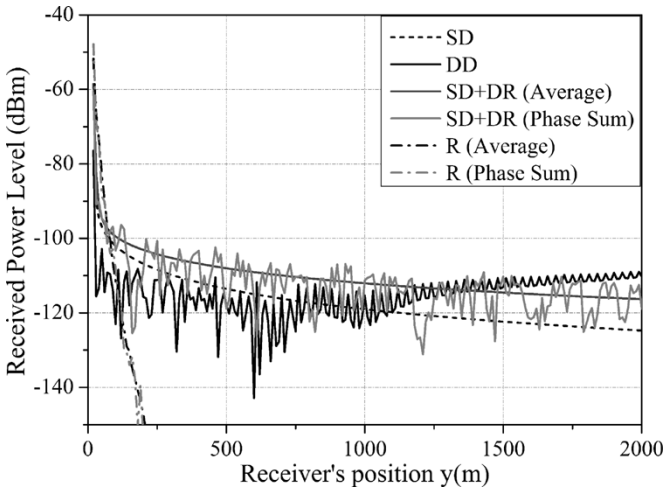

Fig. 6. Received power level (dBm) along path B for different propagation mechanisms and the transmitter placed below rooftop level.

The acronyms of the examined propagation mechanisms are summarized in Table I.

For the double diffraction, only the wedges with axes parallel to wedge a are considered, due to the polarization of the EM waves after the 1st diffraction. A ray-tracing algorithm is implemented, in order to identify all possible multiply reflected paths, by applying an image method. After calculating the complex reflection coefficients, the magnitude and phase of each propagating component is determined. The dielectric constant for all lossy materials is considered complex [26].

In correspondence to Fig. 4, the transmitter was placed at distance $d_T = 200$ m from corner a. Following the "Mediterranean" urban style, the street's width was set to $d_B = 20$ m, and the buildings' height to $h_B = 30$ m. The spacing among successive wedges with perpendicular axes was set to $d_v = 10$ m. Different geometries that better approximate the geometrical characteristics of other environments (Manhattan or Northern European style) are also investigated in the following paragraphs. The transmitter is placed below the surrounding buildings at height $h_T = 10$ m and the receiver at height $h_R = 2$ m. The transmission of a single carrier at $f = 1800$ MHz at a power of $W_T = 1$ W is considered. The transmitter is a vertically polarized $\lambda/2$ dipole antenna, while the receiver is a linear co-polarized elementary dipole. For the results shown in Fig. 6, we have considered $\varepsilon_r = 6.05$ and $\tan\delta = 0.27$ [25], [27], corresponding to concrete with 0% moisture. Similar calculations were repeated for various other usual construction materials, [22], [28]. Similar results were obtained to those presented

in Fig. 6 with all the curves shifted by a constant factor. The receiver is moving along path B at the center of the street from the initial NLOS position for a total distance of $d_R = 2020$ m [2000 m from the corner a—Fig. 4(b)] along the y axis. The received power from each of the aforementioned propagation mechanisms is calculated at 10 m intervals along the y axis. For each position, the total field results by vectorially summing the individual multipath components that reach the receiver with various magnitudes and phases, due to the various propagation paths and mechanisms involved; this is represented in the graphs as "phase sum"

$$P = \frac{\lambda^2}{4\pi}\frac{1}{2\eta}\left|\sum_i G_R(\theta_i,\phi_i)E_i e^{ja_i}\right|^2 \tag{3}$$

where λ is the wavelength of operation, η the characteristic impedance of free-space, φ_i, θ_i the angle of arrival of component i, measured at a spherical coordinate system centered at the receiver, $G_R(\theta_i,\varphi_i)$ the corresponding receiver's gain, E_i the magnitude of the electric field of component i, and a_i its phase.

Given that the phases of the multipath components are considered random variables uniformly distributed in $(0, 2\pi)$, the average received power $\hat{P}$, plotted in our results, is proportional to the sum of the square of the electric field of the individual components:

$$\hat{P} = \frac{\lambda^2}{4\pi}\frac{1}{2\eta}\sum_i \left(G_R(\theta_i,\phi_i)E_i\right)^2 \tag{4}$$

where $\hat{P}$ is represented in the plots as "Average." As can be observed in Fig. 6, the resulting field due to the multiple reflections (R) is strong for distances very close to the corner and then it degrades rapidly. The sum of the singly diffracted (SD) field with the diffracted multiply-reflected field (SD+DR) dominates at distances from 50 m to 1200 m. The doubly diffracted (DD) field, from the array of wedges with perpendicular axes, becomes dominant after 1200 m. Moreover, a clear reduction of the fast fading pattern of the DD field is observed. This implies a strong phase correlation of the individual multipath components at greater distances, which may also explain the observed signal-strength rise. This interesting, but unexpected, field rise is addressed analytically below.

1) Power Level of the Doubly Diffracted EM Waves, Received at a Fixed Location: The receiver is considered at $d_R = 1300$ m ($y = 1300$ m in Fig. 5). In Fig. 7, the power that reaches the receiver after each DD path of Fig. 5 is analyzed. The x-axis represents the y coordinate of each wedge at the right of the receiver, where the 2nd diffraction occurs. The successive wedges at the right of the receiver are treated as a pair and the resultant field is calculated. For each path, we plot the incident power at corner a, the incident power at the 2nd wedge, after the 1st diffraction at corner a, and the power that reaches the receiver. The SD power is also plotted for reference (dashed line). The main part of the energy arrives from the wedges between the receiver and corner a. In that region, the lengths of the paths of all the multipath components become comparable, due to the narrow width of the street compared to the distance of the receiver from the 1st wedge. As

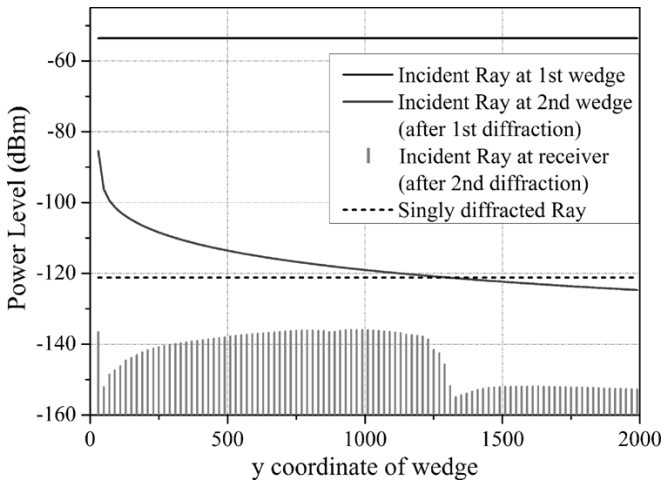

Fig. 7. Analysis of the power level (dBm) for a fixed position at $y = 1300$ m for each double diffraction path (calculation of the power at each wedge and at the receiver).

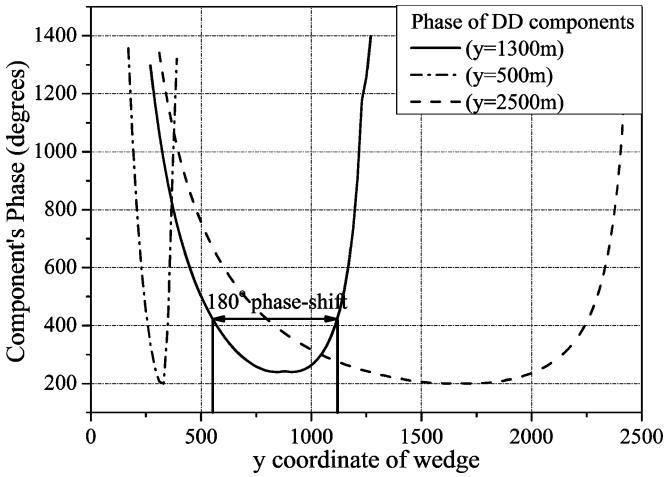

Fig. 8. Phase of each DD component for 3 receiver's positions.

a consequence, they arrive with similar phases at the receiver and contribute constructively to the overall field. As shown in Fig. 8 (continuous line), phases of all arriving components from facades that extended within approximately 600 m vary just by π. As a consequence, the overall DD field becomes greater than the SD one. As the distance between the receiver and corner a grows, the length of the facades from which the DD components add constructively at the receiver increases. Therefore, the DD field is expected to be dominant at greater distances. Two additional examples for a receiver placed at 500 m and 2500 m are given in Fig. 8 with the corresponding "active" facade lengths.

Next, we present the evolution of the DD field along path B of Fig. 4(b) as a function of the geometry of the surrounding environment.

2) Variation of the Linear Density of the Wedges: The spatial density of the wedges is entirely related to the site-specific urban style. It should be chosen according to the number of the "architectural" features along a building's facade. As the linear density grows, the overall field at the receiver is expected to rise. This behavior is depicted in Fig. 9, where four different cases of

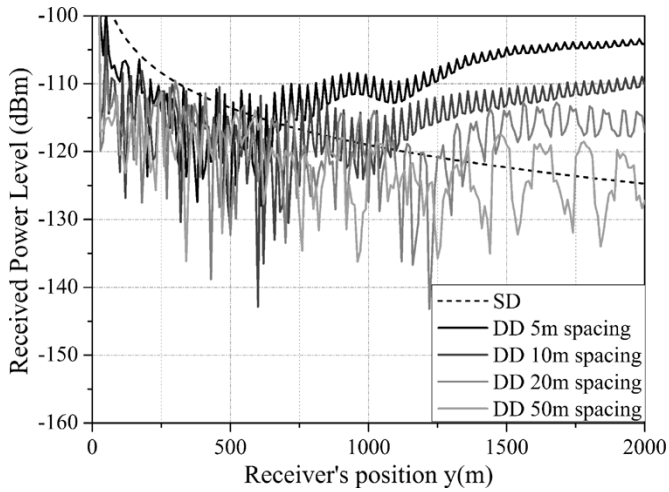

Fig. 9. Received power level along path B for different spacing (linear density) among successive wedges.

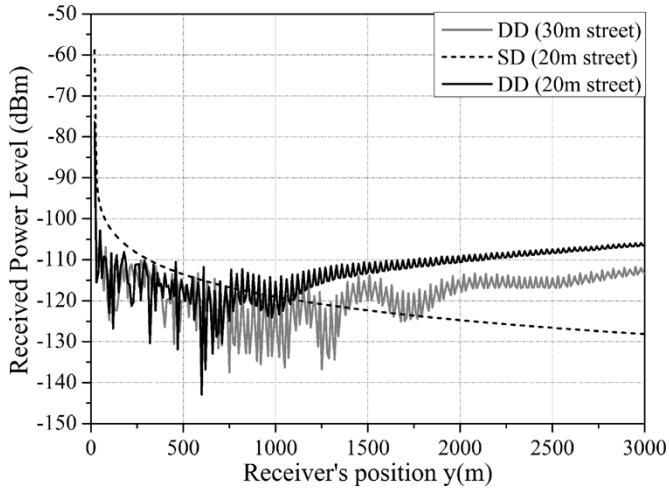

Fig. 10. Received power level along path B for different street's width.

wedge-spacing are considered (d_v is altered from 5 m to 50 m). The same geometry of Fig. 4(b) is considered. By comparing the cases where $d_v = 5\ \mathrm{m}$ and $d_v = 10\ \mathrm{m}$, it seems that the DD curve preserves its shape. As the spacing grows, the arriving components become less correlated, due to the greater path differences among successive wedges (20 m and 50 m spacing), and therefore the resultant field decreases. In Fig. 9, the SD field is also plotted for reference.

An interesting approach would be to arrange the wedges according to a specific distribution function (e.g., Gaussian). Such a configuration would result in a selective flow of energy toward the receiver, mainly from the areas with increasing scatterers' density. This scenario will be the subject of a future research.

3) Variation of the Street's Width: The spacing d_v among successive wedges is set to 10 m and the DD field is calculated along path B for two cases of street's width ($d_B = 20\ \mathrm{m}$ and $d_B = 30\ \mathrm{m}$). As shown in Fig. 10, the curve that corresponds to the wider street geometry approximates a stretched version of the narrow-street case. A similar shape is repeated at greater distances and at lower power values. For the wider-street case, the path from each wedge becomes longer. The path differences also grow. Hence, multipath components from successive wedges tend to correlate at greater distances. Due to the greater path-lengths the total received field is also lower. Therefore, once the field for a given street's width has been calculated, similar behavior for other widths but at different distances from the initial wedge is expected. This distance depends on the ratio of the street widths.

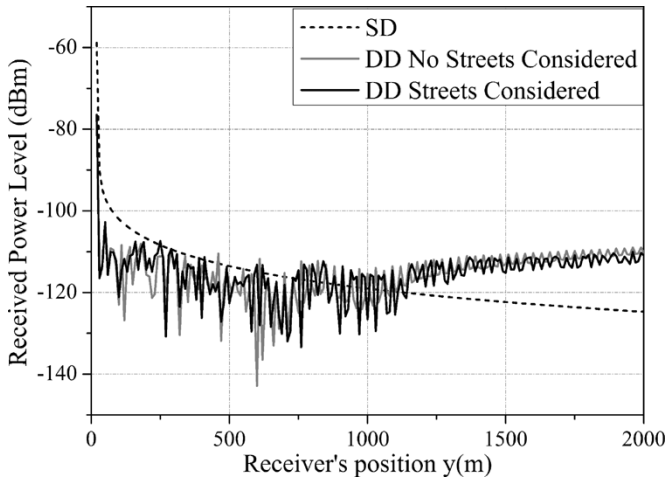

Fig. 11. Comparative diagram for the received DD power level along path B with and without the side streets.

4) Side Streets: In the analysis so far, a continuous structure surrounding path B has been considered. Now, the case represented in Fig. 4(a) will be examined, where streets vertical to path B exist and part of the incident energy is guided to them. Each building's length is considered 50 m and the street's width 20 m. The other geometrical parameters remain as in the case of Fig. 6. The DD field is calculated along path B and plotted in Fig. 11. The corresponding field of the previous case and the SD field from wedge a are also plotted for reference. The existence of the side streets seems to barely affect the total DD field at longer distances. The overall power is diminished, but the curve preserves its initial shape. At greater distances, this fall is proportional to the ratio of the building to the street length (in this case 5/7, resulting in 1.4 dB fall).

In Fig. 12, the average diffracted, multiply-reflected (SD+DR) field is plotted considering also the side streets. The singly diffracted field SD and the SD+DR field of the previous case are plotted for reference. The SD+DR field fades along path B, reaching the SD level, due to the inexistence of the multiply-reflected focusing paths.

Calculation of the Doubly Diffracted Field at Greater Distances: Fig. 13 presents the DD field after a distance of 2 km from the 1st wedge. The wedges along the buildings' facades are arranged at 10 m intervals from $y = 1000\ \mathrm{m}$ to $y = 2000\ \mathrm{m}$ (Fig. 13). In the same graph, the SD and SD+DR field are given for reference. The DD field still remains dominant for larger distances. It begins to decrease at about 2.5 km from the 1st wedge and then follows the same slope as the SD curve.

For various facade intervals or lengths, the DD component is expected to follow similar behavior with a maximum value at another position.

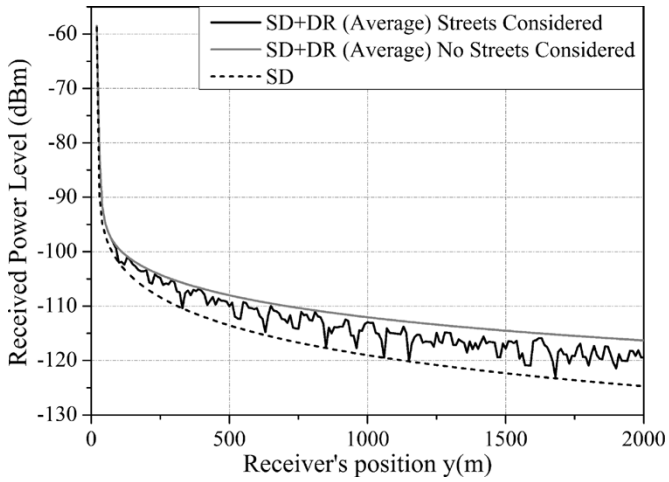

Fig. 12. Comparative diagram for the received (SD+DR) power level along path B with and without the side streets.

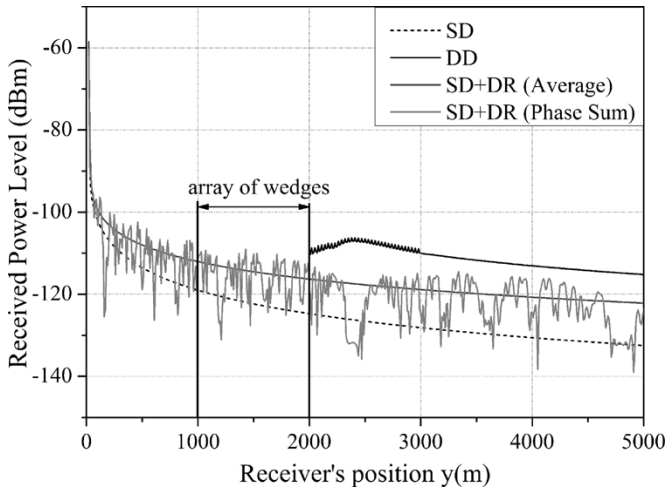

Fig. 13. Received power level along path B for larger distances from the initial wedge.

B. Transmitter Placed Above Rooftop Level

The same typical urban geometry, shown in Fig. 4, will be considered. The transmitter is placed at a horizontal distance $d_T = 500\,\mathrm{m}$ from wedge a, above the surrounding rooftops at a height $h_T = 45\,\mathrm{m}$. The area surrounding path B is substituted with a continuous structure, as shown in Fig. 4(b). The following parameters are set (Fig. 4): $d_B = 20\,\mathrm{m}$, $h_B = 30\,\mathrm{m}$, receiver's height $h_R = 2\,\mathrm{m}$, $f = 1800\,\mathrm{MHz}$, $W_T = 1\,\mathrm{W}$. The transmitter is a vertically polarized $\lambda/2$ dipole antenna, while the receiver is a perfect isotropic antenna, in order to avoid any influence of the radiation pattern of a directional antenna to our conclusions. The structure's facade is replaced with two orthogonal sets of wedges with axes parallel and vertical to the ground, following the procedure described in Section II and depicted in Figs. 2, 3, and 4(c) and (d). Similarly to the analysis of the previous paragraphs, two alternating types of wedges are considered.

As the receiver moves along path B, the magnitude of the field that reaches the receiver under the following propagation mechanisms is examined: a) after a single diffraction (SD) at the rooftop at the left of path B; b) the SD field of case (a) plus the multiply reflected rays at the surfaces of the structure

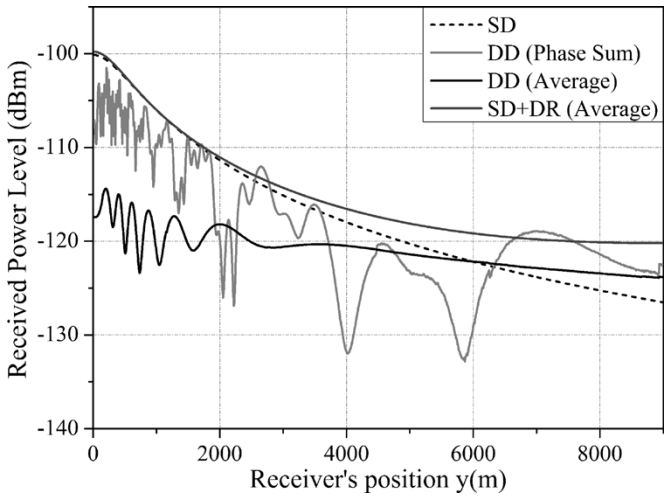

Fig. 14. Received power level (dBm) along path B for different propagation mechanisms and the transmitter placed above rooftop level.

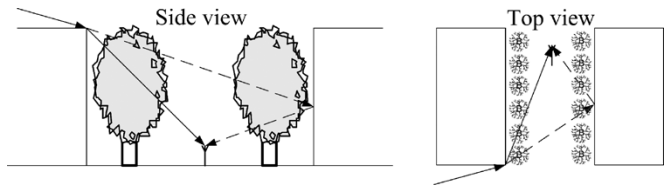

Fig. 15. Representation of the considered arrangement of trees.

that surrounds path B after the initial diffraction (DR); and c) the doubly diffracted rays (DD) that reach the receiver after being diffracted at the rooftop at the left side of path B. Then, those rays are additionally diffracted at each one of the series of wedges having axes parallel to the ground at the buildings' facade at the right side of path B. Similarly to the previous analysis, only the wedges with horizontal axes are considered due to the polarization of the EM waves after the 1st diffraction.

The evolution of the above components is shown in Fig. 14. The field is calculated at 10 m intervals. The distance d_p is set to 1.5 m, which corresponds to a pair of wedges per floor for a 3 m typical floor height. The horizontal axis of Fig. 15 represents the position of the transmitter along the y axis of Fig. 4(b). For better visualization, only $\widehat{P}_{SD+DR}$ is demonstrated. For $\widehat{P}_{DD}$, (3) is initially implemented to calculate the DD field that reaches the receiver from each pair of wedges and the results are introduced in (4). $\widehat{P}_{DD}$ decreases at a different slope than P_{SD} and becomes greater at about 6 km from corner a [Fig. 4(b)]. $\widehat{P}_{SD+DR}$ is dominant in the entire area and follows a similar slope to that of the DD case after the 5th km. The slowly-varying changes in P_{DD} reveal phase-correlation among successive receiver's positions.

C. Effects of Foliage

In the urban environment, trees are typically aligned next to the buildings, as shown in Fig. 15. In this part, the effect of the roadside foliage in the DD paths is examined. It will be shown that the resultant attenuation is greater for the DD rays, compared to the SD ones.

Attenuation of the incident field (in dB/m through foliage) depends on the frequency, the angle of incidence, its polarization,

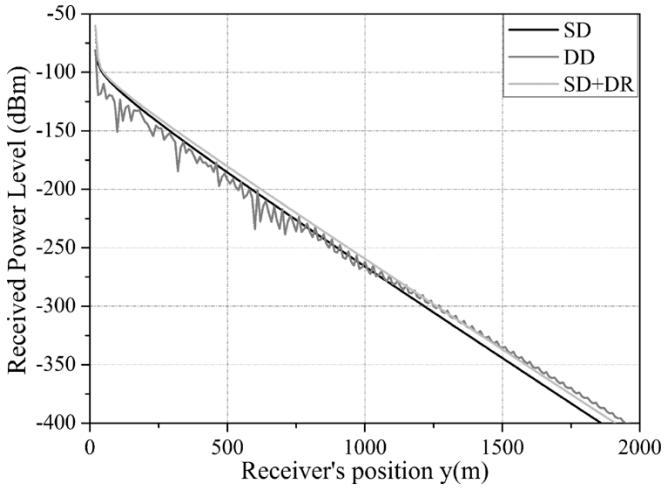

Fig. 16. Received power level for the different propagation mechanisms upon consideration of roadside foliage.

the type of tree [29]–[31] and the season. For the calculations, constant attenuation $a = 0.5\ (\mathrm{dB/m})$ is considered, regardless of the incident angle (Fig. 15). Therefore, the overall attenuation imposed by the trees for a given path depends solely on the distance traveled through them. The received power level from different propagation mechanisms is calculated, with the typical configuration of Fig. 15. The width of the row of trees is considered 3 m and the height of the trees equal to that of the surrounding buildings (30 m). We have not considered any randomness to the phases of the arriving components at the receiver that the foliage is expected to induce. This would further reduce the total strength of the DD field, eliminating the long-distance phase correlation.

The results are plotted in Fig. 16. The received field from all propagation mechanisms degrades rapidly. The SD ray alone describes adequately the overall path loss along path B. The other mechanisms (SD+DR and DD) are not dominant, due to the greater distance traveled through vegetation compared to the previous one. Bearing in mind also the results of Figs. 6 and 12, the SD field represents a secure minimum of the expected signal strength, which may be considered as a safe lower level for sufficient cell-coverage design. The results are similar for the case of the transmitter placed above rooftop level.

V. Experimental Results

We measured the received signal strength in two typical urban canyons in Thessaloniki, Greece, in order to investigate the validity of the predicted wave-guiding behavior. A carrier frequency of 2 GHz was transmitted at 22 dBm. An averaging procedure was followed at the receiver for each measurement sample. In both cases, the transmitting and the receiving antennas were placed below rooftop level. The former was set at 6 m above the ground. The latter was placed on top of a moving vehicle at 3 m above the ground. The antennas used, have 7.5 dBi gain, and are manufactured by Huber-Suhner (model 1319.26.0024). The measurements were carried out early on a Sunday morning, in order to ensure relatively low traffic conditions.

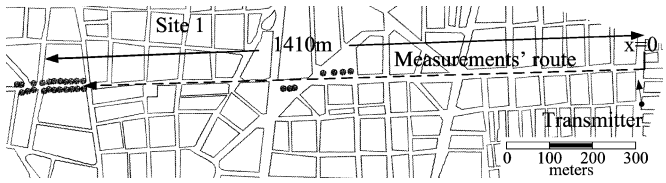

Fig. 17. Map of the area around the 1st set of measurements.

Fig. 18. Photograph of the measurements' route of site 1, taken from the LOS crossroad.

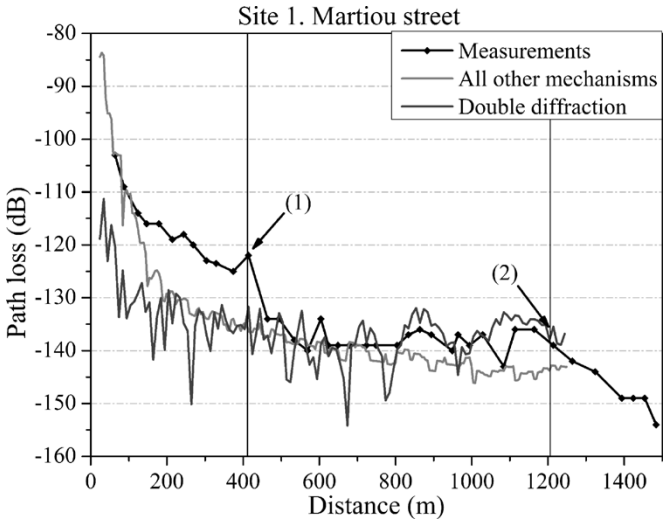

Fig. 19. Experimental results and prediction at increasing distance from the LOS crossroad for site 1.

A. Site 1

The 1st set of measurements was conducted at Martiou street, as represented in Fig. 17. The samples were taken along a straight path, at the center of the street, for a total distance of approximately 1400 m. The street's width is 24 m. The transmitter was placed at a distance of 85 m from the measurements' route. The areas with roadside trees are also shown in Fig. 17. A photo of the street, taken at the beginning of the route, is shown in Fig. 18. The results are given in Fig. 19, along with the predicted doubly diffracted field and the average field from all other mechanisms (multiple reflections, diffraction-reflections). The total field from all mechanisms generally followed the maximum of the two curves ($\mathrm{Total\ field} \approx \max\{\mathrm{All\ other\ mechs,\ DD}\}$). This curve is not included in the results to ensure clarity of the DD field. For the predicted field, the actual geometry was simulated. For the set of wedges on the concrete walls of the buildings, we

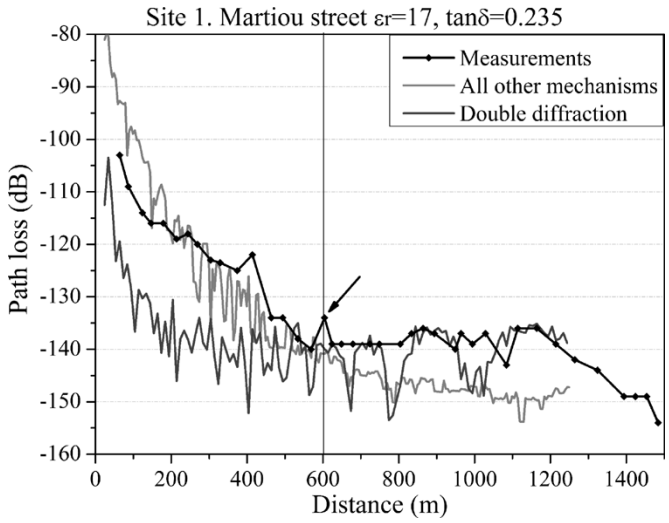

Fig. 20. Experimental results and prediction for site 1 for reflection coefficient, corresponding to 30% moisture.

have considered $\varepsilon_r = 6.05$ and $\tan\delta = 0.27$ (0% moisture). The spacing among successive wedges along the facades of the buildings was set to 2 m. This value was selected based on the actual architectural characteristics of the buildings.

In the area of interest, between 400 m and 1200 m, a clear wave guiding behavior was recorded. In fact, the DD field seems to accurately match the measured path loss profile. Both curves exhibit the same local maxima at 870 m and 1100 m. The other mechanisms fail to predict this behavior. After 1200 m, the receiver enters the area with trees, as shown in Fig. 17, and the received field falls rapidly.

For shorter distances (150 m–400 m), the measured field is 3 to 10 dB stronger than the predicted one. At these distances, where the term describing the multiply reflected field dominates, the measured field decreases also with a different slope than the predictions. The slope of this term depends on the reflection coefficients, which in turn depend on the building materials. This strongly indicates that the actual constitutive parameters of the buildings in the propagation area during the measurements were different than the theoretical. The measurements were performed a few hours after a rainfall. As expected, part of the water was absorbed by the concrete walls of the buildings, changing their complex permittivity. According to [32], the real part of the complex permittivity of concrete can vary from 5 to 17 as the absorbed water volume changes from 0% to 30%, while the imaginary part from 0.5 to 4 respectively (for 0% water volume) at 3 GHz. By corresponding the constitutive parameters of the materials to 30% moisture ($\varepsilon_r = 17$, $\tan\delta = 0.235$), the predicted field matches better the measurements, as shown in Fig. 20.

For the new complex permittivity, the predictions approximate the measurements at all distances. The waveguiding behavior after 600 m from the LOS crossroad is again well predicted by the DD mechanism. At great distances (more than 1000 m), all other mechanisms are 15 dB lower than the measured values.

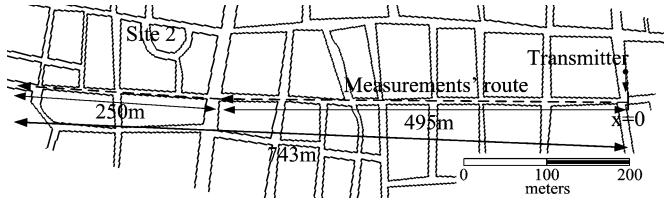

Fig. 21. Map of the area around the 2nd set of measurements.

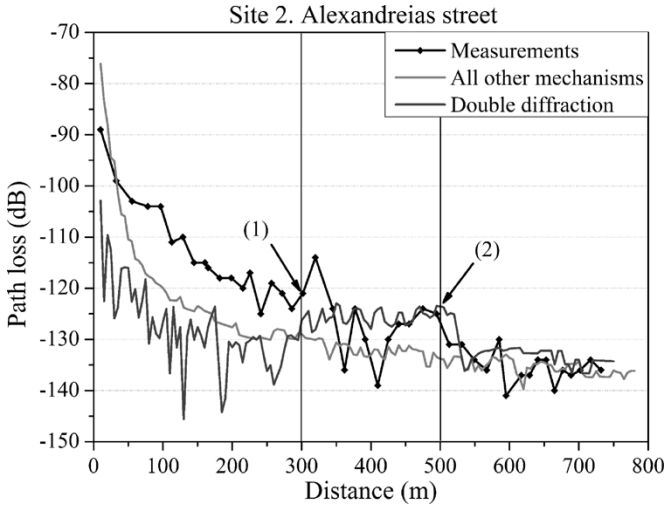

Fig. 22. Experimental results and prediction at increasing distance from the LOS crossroad for site 2.

B. Site 2

The 2nd set of measurements was carried out at Alexandreias Sreet. This is a very narrow street (10 m width) with a small turn at 495 m, as shown in Fig. 21. Similar buildings are located around the receiver. Hence, the wedges along the buildings' facades were again considered at 2 m intervals. The transmitting antenna was placed 40 m from the measurements' route.

As shown in Fig. 22, the measured field behaves similarly for small distances, around the LOS corner, remaining greater than the prediction between 100 m and 300 m, for the same reasons explained in the previous case (0% moisture). Once again, from 300 m to 500 m, the wave-guiding behavior, predicted by the DD field, was verified. The two curves reach their local maxima around 500 m. Then, both the measured and the predicted fields fall at a lower level, as expected due to the slight turning of the street. The predictions match the measured samples until the end of the path.

VI. Conclusion

In this paper, the influence of "urban" scatterers located along buildings' facades was examined. We demonstrated that these discontinuities, so far neglected by existing models, are significant for the microwave frequencies where current wireless communications operate. Since the announced future wireless systems will operate at even higher frequencies, our thesis will be even more important.

In the case that a transmitter is located below rooftop level, it was shown both in theory and experimentally, that the scattered field from the buildings' facades may become important or even dominant at greater distances from the transmitter. Compared to other propagation mechanisms (multiple reflections), the observed wave-guiding behavior is almost unaffected by the side-streets. We have demonstrated how the magnitude of this field varies with the density of the scatterers along the buildings' facades and the geometry of the specific environment.

In the case that a transmitter is located above rooftop level, the received scattered field strength becomes comparable to the one received from the other propagation mechanisms at greater distances and contributes complementary in the total received power.

In all the examined cases, the singly diffracted field represents a safe expected minimum of the received power level.

We have additionally focused in providing a way to model the facade of the buildings in a subtractive and EM significant way. We believe that an extra degree of freedom has been put forward in modeling urban propagation. The idea of deconstructing the urban scene into significant elementary descriptive patterns, allows the study of the prevailing propagation modes and their impact to the received signal, and can also be extended to other architectural features, according to the wavelength in use. Such an approach could also facilitate the solution of the inverse problem in the future; that is to geometrically and electromagnetically characterize the urban environment by performing a single measurement.

ACKNOWLEDGMENT

The authors would like to thank Mr. T. Vasiliadis and Dr. S. Siachalou for their assistance in performing the measurements.

REFERENCES

[1] S. Y. Seidel and T. S. Rappaport, "Site-specific propagation prediction for wireless in-building personal communication system design," *IEEE Trans. Veh. Technol.*, vol. 43, no. 4, Nov. 1994.

[2] M. C. Lawton and J. P. McGeehan, "The application of a deterministic ray launching algorithm for the prediction of radio channel characteristics in small-cell environments," *IEEE Trans. Veh. Technol.*, vol. 43, no. 4, Nov. 1994.

[3] G. Liang and H. L. Bertoni, "A new approach to 3-D ray tracing for propagation prediction in cities," *IEEE Trans. Antennas Propag.*, vol. 46, no. 6, pp. 853–863, Jun. 1998.

[4] W. Zhang, "Fast two-dimensional diffraction modeling for site-specific propagation prediction in urban microcellular environments," *IEEE Trans. Veh. Technol.*, vol. 49, no. 2, pp. 428–436, Mar. 2000.

[5] T. K. Sarkar, Z. Ji, K. Kim, A. Medour, and M. Salazar-Palma, "A survey of various propagation models for mobile communications," *IEEE Antennas Propag. Mag.*, vol. 45, no. 3, pp. 51–82, Jun. 2003.

[6] J. B. Keller, "Geometrical theory of diffraction," *J. Opt. Soc. Amer.*, vol. 52, no. 2, pp. 116–130, Feb. 1962.

[7] R. G. Kouyoumjian and P. H. Pathak, "A uniform geometrical theory of diffraction for an edge in a perfectly conducting surface," *Proc. IEEE*, vol. 62, no. 11, pp. 1448–1461, Nov. 1974.

[8] W. D. Burnside and K. W. Burgener, "High frequency scattering by a thin lossless dielectric slab," *IEEE Trans. Antennas Propag.*, vol. 31, no. 1, pp. 104–110, Jan. 1983.

[9] R. J. Luebbers, "Finite conductivity uniform GTD versus knife edge diffraction in prediction of propagation path loss," *IEEE Trans. Antennas Propag.*, vol. 32, no. 1, pp. 70–76, Jan. 1984.

[10] J. B. Andersen, "UTD multiple-edge transition zone diffraction," *IEEE Trans. Antennas Propag.*, vol. 45, no. 7, pp. 1093–1097, Jul. 1997.

[11] K. Rizk, R. Valenzuela, D. Chizhik, and F. Gardiol, "Application of the slope diffraction method for urban microwave propagation prediction," in *Proc. 48th IEEE VTC*, vol. 2, May 1998, pp. 1150–1155.

[12] C. Tzaras and S. R. Saunders, "An improved heuristic UTD solution for multiple-edge transition zone diffraction," *IEEE Trans. Antennas Propag.*, vol. 49, no. 12, pp. 1678–1682, Dec. 2001.

[13] L. E. Vogler, "An attenuation function for multiple knife-edge diffraction," *Radio Sci.*, vol. 17, no. 6, pp. 1541–1546, Nov./Dec. 1982.

[14] M. Albani, F. Capolino, S. Maci, and R. Tiberio, "Diffraction at a thick screen including corrugations on the top face," *IEEE Trans. Antennas Propag.*, vol. 45, no. 2, pp. 277–283, Feb. 1997.

[15] F. Capolino, M. Albani, S. Maci, and R. Tiberio, "Double diffraction at a pair of coplanar skew edges," *IEEE Trans. Antennas Propag.*, vol. 45, no. 8, pp. 1219–1226, Aug. 1997.

[16] D. Erricolo and P. L. E. Uslenghi, "Two-dimensional simulator for propagation in urban environments," *IEEE Trans. Veh. Technol.*, vol. 50, no. 4, pp. 1158–1168, Jul. 2001.

[17] M. Albani, "A uniform double diffraction coefficient for a pair of wedges in arbitrary configuration," *IEEE Trans. Antennas Propag.*, vol. 53, no. 2, pp. 702–710, Feb. 2005.

[18] P. D. Holm, "UTD-diffraction coefficients for higher order wedge diffracted fields," *IEEE Trans. Antennas Propag.*, vol. 44, no. 6, pp. 879–888, Jun. 1996.

[19] D. Erricolo, "Experimental validation of second-order diffraction coefficients for computation of path-loss past buildings," *IEEE Trans. Electromag. Compat.*, vol. 44, no. 1, pp. 272–273, Feb. 2002.

[20] A. J. Goldsmith and L. J. Greenstein, "A measurement-based model for predicting coverage areas of urban microcells," *IEEE J. Select. Areas Commun.*, vol. 11, no. 7, pp. 1013–1023, Sep. 1993.

[21] V. Erceg, A. J. Rustako, and P. S. Roman, "Diffraction around corners and its effects on the microcell coverage area in urban and suburban environments at 900 MHz, 2 GHz, and 6 GHz," *IEEE Trans. Veh. Technol.*, vol. 43, no. 3, pp. 762–766, Aug. 1994.

[22] S. R. Saunders, *Antennas and Propagation for Wireless Communication Systems*. New York: Wiley, 1999.

[23] J. Walfisch and H. L. Bertoni, "A theoretical model of UHF propagation in urban environements," *IEEE Trans. Antennas Propag.*, vol. 36, no. 12, pp. 1788–1796, Dec. 1988.

[24] L. R. Maciel, H. L. Bertoni, and H. H. Xia, "Unified approach to prediction of propagation over buildings for all ranges of base station antenna height," *IEEE Trans. Veh. Technol.*, vol. 42, no. 1, pp. 41–45, Feb. 1993.

[25] M. F. Catedra and J. Perez-Arriaga, *Cell Planning for Wireless Communications*. Boston, MA: Artech House, 1999.

[26] A. Von Hippel, *Dielectric Materials and Applications*. Boston, MA: Artech House, 1995.

[27] C. K. Sou, O. Landron, and M. J. Feuerstein, "Characterization of electromagnetic properties of building materials for use in site-specific propagation prediction," Virginia Tech, Mob. Port. Radio Res. Group Tech. 92-12, 1992.

[28] ITU, Recommendation ITU-R P. 1238-2, Feb. 2001.

[29] S. A. Torrico, H. L. Bertoni, and R. H. Lang, "Modeling tree effects on path loss in a residential environment," *IEEE Trans. Antennas Propag.*, vol. 46, no. 6, Jun. 1998.

[30] W. J. Vogel and J. Goldhirsch, "Tree attenuation at 869 MHz derived from remotely piloted aircraft measurements," *IEEE Trans. Antennas Propag.*, vol. 34, no. 12, pp. 1460–1464, Dec. 1986.

[31] J. Goldhirsch and W. J. Vogel, "Roadside tree attenuation measurements at UHF for land mobile satellite systems," *IEEE Trans. Antennas Propag.*, vol. 35, no. 5, pp. 589–596, May 1987.

[32] J. B. Hasted and M. A. Shah, "Microwave absorption by water in building materials," *British J. Appl. Phys.*, vol. 15, pp. 825–836, 1964.

Antonis G. Dimitriou (S'01) was born in Ierapetra, Greece, in 1977. He received the Diploma in electrical and computer engineering from the Aristotle University of Thessaloniki, Greece, in 2001, where he is working toward the Ph.D. degree.

Since 2001, he has been a Teaching and Research Assistant in the Department of Electrical and Computer Engineering of the Aristotle University of Thessaloniki, where he has participated in numerous research activities, including the design of a GSM cellular network inside the Olympic Stadium for the 2004 Olympic Games. His current interests are in the areas of antennas, propagation modeling, using high frequency methods in electromagnetics and planning.

Mr. Dimitriou is a member of the Technical Chamber of Greece.

George D. Sergiadis (M'88) was born in Thessaloniki, Greece, in 1955. He received the Diploma degree in electrical engineering from the Aristotle University of Thessaloniki, Thessaloniki, Greece, in 1978, and the Ph.D. degree from "Ecole Nationale Supérieure des Télécommunications," Paris, France, in 1982.

He worked with Thomson CsF, in France, until 1985, participating in the development of the French Magnetic Resonance Scanner. Since 1985, he has been with the Aristotle University of Thessaloniki, Greece, teaching telecommunications and biomedical engineering, where he is currently an Associate Professor. For three years he also served as the Director of the Telecommunications Department. He has developed the Hellenic TTS engine "Esopos," and designed the mobile communications for the Athens Olympic Games in 2004. His current research interests include fuzzy image processing and wireless communications. During the academic year 2004–2005 he was a Visiting Researcher at Media Lab, MIT, Cambridge, MA.

Dr. Sergiadis is the president of ELEVIT, the Hellenic Society for Biomedical Engineering, and a member of the Technical Chamber of Greece, ATLAS, SMRM, ESMRM, EMBS, and SCIP.